

Article

New Indirect Tire Pressure Monitoring System Enabled by Adaptive Extended Kalman Filtering of Vehicle Suspension Systems

Dong-Hoon Lee , Dal-Seong Yoon and Gi-Woo Kim * 

Department of Mechanical Engineering, Inha University, Incheon 22212, Korea; dlalid92@naver.com (D.-H.L.); dalsungyoon@gmail.com (D.-S.Y.)

* Correspondence: gwkim@inha.ac.kr

Abstract: This paper presents a new indirect tire pressure monitoring system (TPMS) based on adaptive extended Kalman filtering with unknown input (AEKF-UI) estimation of vehicle suspension systems. The suggested methodology is based on the explicit correlation between tire pressure and tire stiffness and is available in real time. AEKF-UI is used to simultaneously estimate the time-varying parameter (tire stiffness) of vehicle suspension systems and the road roughness using an unknown input estimator. Simulation studies demonstrate that the proposed algorithm can simultaneously estimate tire stiffness (i.e., tire inflation pressure) variation and unknown road roughness input. The feasibility and effectiveness of the proposed estimation algorithm are verified through a laboratory-level experiment. This study offers a potential application for an alternative indirect TPMS and the estimation of unknown road roughness used for automotive controller design.

Keywords: adaptive extended Kalman filter; sensor fusion; time-varying parameter estimation; tire stiffness; tire pressure monitoring system; unknown road roughness input



Citation: Lee, D.-H.; Yoon, D.-S.; Kim, G.-W. New Indirect Tire Pressure Monitoring System Enabled by Adaptive Extended Kalman Filtering of Vehicle Suspension Systems. *Electronics* **2021**, *10*, 1359. <https://doi.org/10.3390/electronics10111359>

Academic Editor:
Mahmut Reyhanoglu

Received: 24 May 2021
Accepted: 5 June 2021
Published: 7 June 2021

Publisher's Note: MDPI stays neutral with regard to jurisdictional claims in published maps and institutional affiliations.



Copyright: © 2021 by the authors. Licensee MDPI, Basel, Switzerland. This article is an open access article distributed under the terms and conditions of the Creative Commons Attribution (CC BY) license (<https://creativecommons.org/licenses/by/4.0/>).

1. Introduction

Tire pressure can significantly affect vehicle stability and fuel consumption. Therefore, the electronic tire pressure monitoring system (TPMS) used to monitor tire inflation pressure (nominally 32–35 psi), is rapidly becoming an essential electronic system in most vehicles. The National Highway Transport Safety Administration (NHTSA) started investigation on the implementation of tire pressure warning systems in vehicles and stipulated that since 2008, all passenger cars and trucks manufactured in or imported into the United States are required to be equipped with TPMS. For every 0.2 bar under normal inflation levels, fuel consumption can increase and the tire lifetime can decrease by 20% [1]. Furthermore, a lower tire pressure significantly affects pavement damage and decreases the fatigue life of the asphalt surface layers by up to 200% and 300%, respectively [2]. Therefore, TPMS is required not only for vehicle performance, including safety, ride quality and fuel economy, but also for pavement maintenance.

There are two classes of TPMS: direct and indirect. Direct tire pressure monitoring systems have physical pressure sensors mounted on the rim of each tire. An on-board radio-frequency receiver communicates with the TPMS unit and accurately displays the real-time tire pressure. This direct-type TPMS is used in the majority of vehicles available on the market today owing to its high precision. Many researchers have attempted to improve the performance of TPMS, with a primary focus on the use of robust pressure sensor, antenna design and lower power consumption [3]. However, this approach has some technical limitations. For example, additional electronic hardware generally includes an embedded pressure sensor, an analog-to-digital converter, a microcontroller, a wireless transceiver and a battery management system. Many researchers have attempted energy harvesting systems to overcome the battery issue in direct TPMS [4,5]. In contrast to

direct TPMS, indirect TPMS uses software algorithms with existing sensors of the vehicle (frequently referred to as sensor fusion). For example, the resonant frequency of the wheel speed can be used to monitor the tire pressure, as it correlates with tire pressure [6,7], and wheel radius analysis using a sensor fusion technique that receives signals from the anti-lock brake system has been developed based on the fact that the tire internal pressure affects the effective rolling radius of the tire. Isermann et al. developed a new indirect method based on a static nonlinear transformation of wheel speeds [8]. A self-adaptive nonlinear filter with an optimal finite impulse response (FIR) derivative was designed to estimate the tire longitudinal stiffness related to the tire pressure [9]. Marton et al. studied frequency analysis-based tire pressure monitoring [10]. However, although these indirect TPMS increases the inherent advantages, such as no requirement for additional pressure sensor implementations, and have shown promising results, there are no commercialized products based on indirect TPMS to date because there is still room for improvement in terms of accuracy and reliability.

Therefore, the main objective of this study is to explore a new TPMS aimed at addressing the abovementioned issues of existing indirect TPMS. To achieve this research goal, adaptive extended Kalman filtering with unknown input (AEKF-UI) estimation of vehicle suspension systems is proposed for the new indirect-type TPMS in this study. After estimating the time-varying parameter of tire stiffness, the linear static relationship between the tire stiffness and inflation pressure is utilized to indirectly monitor the tire inflation pressure, as shown in Figure 1. While a vehicle drives on a road, the road acts as an unknown disturbance input to the vehicle suspension system. Thus, it is necessary to simultaneously estimate unknown road roughness input. In this study, road roughness can be obtained through the proposed algorithm. Compared with current indirect TPMS, the proposed system can simultaneously monitor the tire pressure (after estimating the tire stiffness) and estimate the unknown road roughness input. This is one of the advantages of the proposed method, because the measurement of road roughness is significant for understanding vehicle dynamics and for designing automotive control systems, but is typically challenging [11]. Furthermore, the proposed algorithm is more accurate and reliable because it is based on vehicle vertical dynamics, whereas most previous indirect TPMS methods suffer from inaccuracy due to the absence of a proper vehicle dynamic model. The quarter-car suspension model and the static relationship between the tire stiffness and inflation pressure are described in Section 2. The proposed algorithm and forgetting factor adjustment are described in Section 3. The simulation and experimental validation are presented in Sections 4 and 5, respectively.

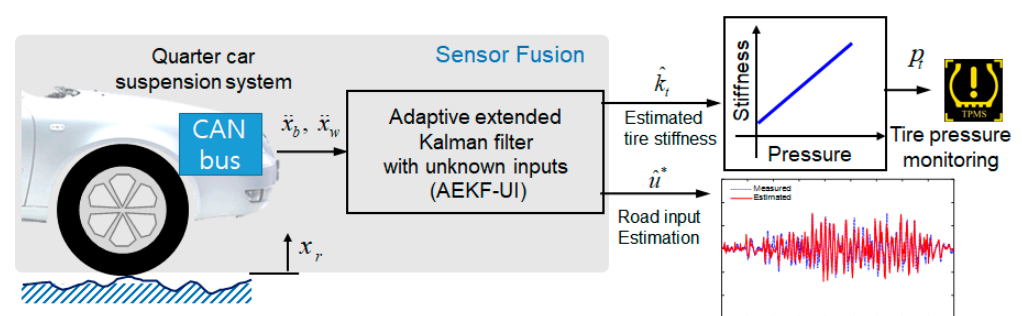


Figure 1. Overview of new indirect TPMS enabled by adaptive extended Kalman filtering of vehicle suspension systems.

2. Quarter-Car Suspension System

Various vehicle models have been developed for different purposes. Each model's suitability depends on the performance evaluation criteria [12,13]. The quarter-car suspension model is designed in a two degree of freedom manner and primarily focuses on the behavior of the sprung mass (the mass of the vehicle chassis) and the unsprung

mass (the mass of a single wheel, tire and shock absorber), while the tire is modeled as a linear spring (i.e., tire stiffness) in series with an unsprung mass, as illustrated in Figure 2. This model is widely used in various studies to simplify the complexity of algorithms as much as possible while ensuring critical performance [14]. The fundamental assumption of a linear quarter-car model is to neglect the complex linkage effects, whereas a practical suspension system is more complicated from a kinematic point of view [15]. Hence, there is an inevitable model–reality mismatch. Nonetheless, the quarter-car model greatly reduces the complexity of the system, thereby being highly effective for embedded systems as compared with higher-order suspension models [16]. Due to these compelling advantages, many researchers have adopted a quarter-car suspension model for analyzing suspension performance or control and the passive-type quarter-car suspension model is utilized in this study. Road roughness (x_r) acts as an unknown input to be either measured or estimated. In this study, the unknown road input is simultaneously estimated by the proposed algorithm.

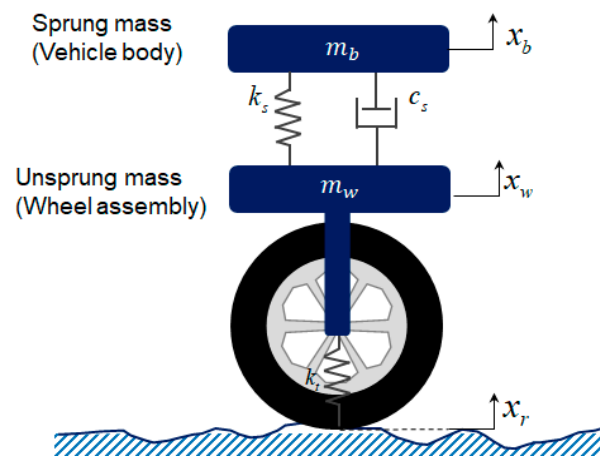


Figure 2. Schematic of quarter-car suspension system consisting of two primary masses (sprung and unsprung).

2.1. State-Space Model of Quarter-Car Suspension Systems

Based on the quarter-car suspension model, the governing equations of a quarter-car suspension model are derived as follows:

$$\begin{aligned} m_b \ddot{x}_b + c_s(\dot{x}_b - \dot{x}_w) + k_s(x_b - x_w) &= 0 \\ m_w \ddot{x}_w + c_s(\dot{x}_w - \dot{x}_b) + k_s(x_w - x_b) + k_t x_w &= k_t x_r \end{aligned} \tag{1}$$

In this study, the unknown time-varying parameter (i.e., tire stiffness) is considered as a state variable and augmented into a state vector such that the equation can be transformed into a nonlinear state equation. Equation (1) can then be expressed by the following nonlinear equation of motion:

$$\mathbf{x} = \begin{bmatrix} x_b & \dot{x}_b & x_w & \dot{x}_w & k_t \end{bmatrix}^T = \begin{bmatrix} x_1 & x_2 & x_3 & x_4 & x_5 \end{bmatrix}^T \tag{2}$$

$u^* = x_r$

$$\begin{aligned} \dot{\mathbf{x}} &= \begin{bmatrix} \dot{x}_1 \\ \dot{x}_2 \\ \dot{x}_3 \\ \dot{x}_4 \\ \dot{x}_5 \end{bmatrix} = \begin{bmatrix} \frac{k_s(x_3 - x_1) + c_s(x_4 - x_2)}{m_b} \\ x_4 \\ \frac{k_s(x_1 - x_3) + c_s(x_2 - x_4) + x_5(x_r - x_3)}{m_w} \\ 0 \\ 0 \end{bmatrix} \\ \mathbf{y} &= \begin{bmatrix} \ddot{x}_b \\ \ddot{x}_w \end{bmatrix} = \begin{bmatrix} \frac{k_s(x_3 - x_1) + c_s(x_4 - x_2)}{m_b} \\ \frac{k_s(x_1 - x_3) + c_s(x_2 - x_4) + x_5(x_r - x_3)}{m_w} \end{bmatrix} \end{aligned} \tag{3}$$

where x_b and x_w are the sprung and unsprung mass displacement, respectively; the road roughness (profile elevation) x_r is an unknown input for the system; m_b and m_w denote the sprung and unsprung masses, respectively. Note that the design of extended Kalman filtering is required because two state variables (x_5 and x_3) in (3) are coupled (nonlinear). The suspension system is described by a linear spring of stiffness k_s and a linear damper with a damping constant c_s . The pneumatic tire is modeled by a linear spring of stiffness k_t . The vertical tire stiffness k_t is the unknown parameter, which is modeled as the state variable for random walk model [17]. This state-space model can be represented as a global structure

$$\begin{aligned}\dot{x} &= f(x, u^*, w) \\ y &= h(x, u^*, v)\end{aligned}\quad (4)$$

where x is the state variable vector defined in (3); w is the process noise; v is the measurement noise; f is the system function; u^* is the unknown input for the system; h is the output function; y is the measurable output; \ddot{x}_b and \ddot{x}_w are the sprung and unsprung mass accelerations, respectively. These acceleration signals can be acquired from the controller area network (CAN) bus, which is the central nervous system of a modern vehicle, upon which the majority of intra-vehicular communication takes place [18,19].

2.2. Relationship between Tire Stiffness and Inflation Pressure

The key assumption of the proposed indirect TPMS is that it uses a linear relationship between the tire stiffness and the pressure. To validate the assumption, the vertical tire stiffness with the different tire pressures was measured using a tire test equipment (Flat-trac CT plus, MTS[®] system). Under the normal operation conditions (150 kPa~300 kPa), the relationship between the tire vertical stiffness and pressure exhibited linear characteristics. Typically, a vehicle tire possesses viscoelastic characteristics. However, this has been neglected in this study because the quarter-car suspension model-based TPMS is operated in response to transient inputs [20]. A commercial tire for mid-size passenger cars (type 225/45R17W, Hankook Tire) was used for the experiment. The measurements were recorded five times at different tire pressures and then averaged, as shown in Table 1. The measured vertical tire stiffness was linearly proportional to the internal tire pressure, as shown in Figure 3. The sensitivity curve was estimated using the following regression (curve fitting) formula ($R^2 = 0.998$)

$$y = 713.91x + 60880 \quad (5)$$

where y denotes the tire stiffness k_t (N/m) and x denotes the tire inflation pressure (kPa).

Table 1. Measurement of tire vertical stiffness with different pressure.

Pressure (psi)	Pressure (kPa)	Stiffness (N/m)
27	186.2	193,780
31	213.7	213,450
35	241.3	233,350
39	268.9	252,960
43	296.5	272,440

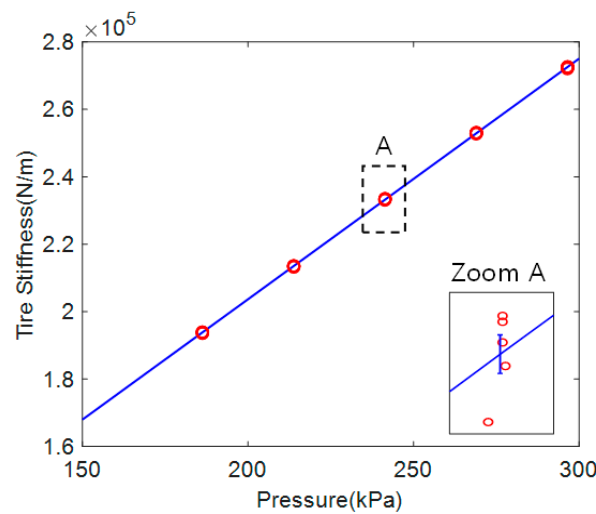


Figure 3. Regression curve from measured pressure vs. tire vertical stiffness (inset: zoomed view).

3. Adaptive Extended Kalman Filter with Unknown Input Estimation

3.1. Overview of EKF Algorithm with Unknown Input Estimation

The terms “dynamic state” and “parameter estimation” can be traced back to the 1970s when Kalman filtering techniques were applied to improve the computational performance of the traditional state estimation process. System modeling and identification methods for nonlinear systems were developed using the extended Kalman filter (EKF). The EKF is an effective means of state and unknown parameter estimation. EKF algorithms can be derived from conventional Kalman filters [21,22]. Yang et al. proposed an extended Kalman filter with unknown input (EKF-UI) to estimate unknown earthquakes for health monitoring of structural systems in the field of civil engineering [23]. The derivation of the EKF-UI is briefly explained as follows:

$$\dot{x}(k) = \frac{x(k) - x(k-1)}{\Delta t} \Rightarrow x(k) = \dot{x}(k)\Delta t + x(k-1) \tag{6}$$

where Δt is the time step; and k and $k - 1$ indicate the time instant at $t = k\Delta t$ and $t = (k - 1)\Delta t$, respectively. Replacing (2) by (6) yields

$$x(k) = x(k-1) + \Delta t \cdot f(x, u^*, w) \tag{7}$$

Equation (7) can be expressed by a different notation as follows:

$$x_k = \Delta t \cdot f(x, u^*, w) + x_{k-1} \tag{8}$$

Equation (8) then becomes the global discrete-time equation as follows:

$$\begin{cases} x_k = f_{k-1}(x_{k-1}, u_{k-1}^*, w_{k-1}) \\ y_k = h_k(x_k, u_k^*, v_k) \end{cases} \tag{9}$$

where $x_k \in \mathbb{R}^{n \times 1}$ is the system state vector, $y_k \in \mathbb{R}^{m \times 1}$ is the measured variable vector, $u_k^* \in \mathbb{R}^{1 \times 1}$ is the unknown input vector, $w_k \in \mathbb{R}^{n \times 1}$ is the process noise; and $v_k \in \mathbb{R}^{m \times 1}$ is the measurement noise vector. It is assumed that the measured sprung mass and the unsprung mass acceleration are sampled at the exact time instant $k \cdot T (k = 0, 1, 2 \dots)$.

$$E[w_k w_j^T] = Q_k \cdot \delta_{kj} \tag{10}$$

$$E[v_k v_j^T] = R_k \cdot \delta_{kj} \tag{11}$$

where δ_k and $E[\cdot]$ denote the Kronecker delta and the expected value operator, respectively. $\{w_k\}$ and $\{v_k\}$ denote sequences of uncorrelated Gaussian random vectors with zero mean; Q_k and R_k represent covariance matrices. The discrete-time EKF-UI algorithm consists of the following steps:

- Initialization of the filter at $k = 0$

$$\begin{cases} \hat{x}_0^+ = E[x_0] \\ \hat{u}_0^* = E[u_0^*] \\ P_0^+ = E[(x_0 - \hat{x}_0^+)(x_0 - \hat{x}_0^+)^T] \\ S_0 = E[(u_0^* - \hat{u}_0^*)(u_0^* - \hat{u}_0^*)^T] \end{cases} \quad (12)$$

- Prediction stage

$$A_{k-1} = \left. \frac{\partial f_{k-1}}{\partial x} \right|_{\hat{x}_{k-1}^+} \quad (13)$$

$$\begin{aligned} \hat{x}_k^- &= f_{k-1}(\hat{x}_{k-1}^+, u_{k-1}^*, 0) \\ P_k^- &= A_{k-1}P_{k-1}^+A_{k-1}^T + Q_{k-1} \end{aligned} \quad (14)$$

The superscript “-” denotes that the estimate is a priori estimate. The prediction stage then updates the state estimate and the estimation-error covariance.

- Unknown input estimation

$$H_k = \left. \frac{\partial h_k}{\partial x} \right|_{\hat{x}_k^-}, D_k^* = \left. \frac{\partial h_k}{\partial u^*} \right|_{\hat{u}_k^*} \quad (15)$$

$$\begin{aligned} K_k &= P_k^- H_k^T (H_k P_k^- H_k^T + R_k)^{-1} \\ S_k &= [D_k^{*T} R_k^{-1} (I - H_k K_k) D_k^*]^{-1} \\ \hat{u}_k^* &= S_k D_k^{*T} R_k^{-1} (I - H_k K_k) \\ &\times [y_k - h(\hat{x}_k^-, \hat{u}_{k-1}^*) + D_k^* \hat{u}_{k-1}^*] \end{aligned} \quad (16)$$

Equation (15) represents a partial derivation matrix of h_k and (16) represents the Kalman gain and unknown input estimation. The superscript “+” denotes a posteriori estimate.

- Correction stage

$$\begin{aligned} \hat{x}_k^+ &= \hat{x}_k^- + K_k [y_k - h(\hat{x}_k^-, \hat{u}_{k-1}^*)] \\ P_k^+ &= [I + K_k D_k^* S_k D_k^{*T} R_k^{-1} H_k] \cdot (I - K_k H_k) P_k^- \end{aligned} \quad (17)$$

Finally, the measurement of the state estimate and estimation-error covariance are updated using (17).

3.2. Adaptive Extended Kalman Filter with Unknown Input

In this study, AEKF-UI with a forgetting factor is proposed to estimate time-varying parameters (tire stiffness) because EKF-UI itself cannot estimate time-varying system parameters. However, a constant forgetting factor does not adaptively weigh the covariance of all states and optimal filtering cannot be assured. As a result, if the forgetting factor is low, it has better tracking capability, but is vulnerable to noise contamination. In contrast, if the forgetting factor is high, it is more robust to noise but has less tracking proficiency. To overcome this problem, the adaptive fading Kalman filter was proposed in [24]. When older data from the current estimate are no longer significant due to the erroneous model associated with parameter uncertainty such as time-varying tire stiffness, the undesirable effects from the erroneous model can be mitigated by the adaptive fading Kalman filter [25,26]. In this study, the adaptive forgetting factor technique was employed to track the time-varying parameters of the vehicle suspension system. To achieve this

goal, the AEKF-UI should be capable of rejecting the effect of older data from a current state erroneous model. As the filter estimation relies heavily on the past data, this may cause the state estimation to diverge. The equations describing the AEKF-UI are identical to those of the EKF-UI in (4)–(16) except for the forgetting factor in the time propagation error covariance equation

$$P_k^- = \lambda_{k-1} A_{k-1} P_{k-1}^+ A_{k-1}^T + Q_{k-1}, \lambda_k \geq 1 \quad (18)$$

Consequently, the influence of the latest measured data in the state and parameter is overweighed and thus divergence is avoided. The performance of the AEKF-UI fully depends on the selection of the forgetting factor. Therefore, the generation of an optimal forgetting factor λ_k is a key problem.

$$z_k = y_k - h(\hat{x}_k^-, \hat{u}_{k-1}^*) \quad (19)$$

The residual, z_k , is a white Gaussian noise sequence. An arbitrary gain K_k in (16) is derived from the following covariance of the residual

$$C_{0,k} = E[z_k z_k^T] = H_k P_k^- H_k^T + R_k \quad (20)$$

To find the optimal Kalman gain, the auto-covariance of the residual is first formulated as follows:

$$\begin{aligned} C_j(k) &= E[z_{k+j} z_k^T] \\ &= H_{k+j} A_{k+j, k+j-1} \\ &\quad \times [I - K_{k+j-1} H_{k+j-1}] \cdots A_{k+2, k+1} \\ &\quad \times [I - K_{k+1} H_{k+1}] A_{k+1, k} \\ &\quad \times [P_k^- H_k^T - K_k C_{0,k}] \quad \forall j = 1, 2, 3, \dots \end{aligned} \quad (21)$$

When (16) and (20) are substituted into (21), $C_{j,k}$ should be zero, which implies that the sequence of residuals is uncorrelated. However, in a practical situation, the real covariance of the residual $C_{0,k}$ will be different from the theoretical one obtained from (16) to (20) because of the error in the model parameters and noise covariance. Typically, the innovation covariance is equal to $C_{0,k}$ when a dynamic equation is exact. However, the exact dynamic equation of a nonlinear stochastic system is not available. Therefore, the estimation error and the predicted error covariance may increase due to the effect of unknown information. Thus, $C_{j,k}$ may not be zero and the forgetting factor should be chosen such that the last term of $C_{j,k}$ in (21) for all $j = 1, 2, 3, \dots$ can be zero

$$P_k^- H_k^T - K_k C_{0,k} = 0 \quad (22)$$

If (22) holds, then the Kalman gain K_k is optimal. This condition forms the basis for adaptive filtering algorithms. The term $C_{0,k}$ in (22) is computed not from (13)–(17) and (20), but from the measured data. T_k and $g_{\lambda,k}$ are also defined as follows:

$$T_k = P_k^- H_k^T - K_k C_{0,k} \quad (23)$$

$$g_{\lambda,k} = \frac{1}{2} \sum_{i=1}^n \sum_{j=1}^m T_{ij,k}^2 \quad (24)$$

The optimality of the Kalman filter can be determined by (24) and $T_{ij,k}^2$ is (i,j) the element of T_k . A smaller g_k implies that the Kalman gain becomes more optimal. Hence, the forgetting factor (λ_k) should be chosen to minimize g_k .

3.3. Forgetting Factor Update

Real-time system identification, least-square estimation (LSE) [26], extended Kalman filter [27] and Monte Carlo filter [28] can be used to identify system parameters. However,

it is difficult to estimate time-varying parameters using these methods because they cannot deal with abrupt parameter changes. Different techniques based on the LSE approach have been proposed to overcome this issue using a constant forgetting factor [29]. As mentioned above, the constant forgetting factor approach has a trade-off between tracking ability and robustness to noise. The forgetting factor should be adaptively updated to identify and track a time-varying parameter based on the following equation:

$$\lambda_k^{l+1} = \lambda_k^l + \varphi \frac{\partial g_{\lambda,k}^l}{\partial \lambda_k^l} \forall l = 0, 1, 2, \dots \quad (25)$$

where the subscript k represents the time series; the superscript l represents the iteration times in a time instant; and φ is the step length (learning rate) in the gradient descent method. At the p -th iteration, if the following condition holds,

$$\left| \lambda_k^p - \lambda_{k-1}^p \right| < \varepsilon \quad (26)$$

The iteration is terminated and the optimal forgetting factor is determined by

$$\lambda_k = \max \{ 1, \lambda_k^p \} \quad (27)$$

However, the iterative computation method fails to achieve an explicit formula for the calculation of λ_k and it is difficult to implement a real-time process. In this study, a one-step AEKF-UI algorithm was employed to resolve this computational issue. Assuming that Q_k , R_k and P_0 are positive definite and that the measurement matrix H_k is full rank, the optimal forgetting factor can be obtained by

$$\lambda_k = \max \{ 1, \text{trace}[N_k] / \text{trace}[M_k] \} \quad (28)$$

where

$$M_k = H_k A_{k,k-1} P_{k-1}^+ A_{k,k-1}^T H_k^T \quad (29)$$

$$N_k = C_{0,k} - H_k Q_{k-1} H_k^T - R_k \quad (30)$$

The forgetting factor can then be estimated using the following three recursive equations with initial conditions $G_{1,0} = 0$ and $G_{2,0} = 0$:

$$C_{0,k} = G_{1,k} / G_{2,k} \quad (31)$$

$$G_{1,k} = G_{1,k-1} / \lambda_{k-1} + z_k z_k^T \quad (32)$$

$$G_{2,k} = G_{2,k-1} / \lambda_{k-1} + 1 \quad (33)$$

Substituting (16) into the optimality condition in (22) yields

$$P_k^- H_k^T \times \left\{ I - [H_k P_k^- H_k^T + R_k]^{-1} C_{0,k} \right\} = 0 \quad (34)$$

$$H_k P_k^- H_k^T = C_{0,k} - R_k \quad (35)$$

Note that (35) implies that the optimality condition in (22) is equivalent to (20). Substituting (18) into (35) yields

$$\begin{aligned} & \lambda_k H_k A_{k,k-1} P_{k-1}^+ A_{k,k-1}^T H_k^T \\ & = C_{0,k} - H_k Q_{k-1} H_k^T - R_k \end{aligned} \quad (36)$$

Simplifying (36) from (29) and (30) yields

$$\lambda_k I = N_k M_k^{-1}, \lambda_k \geq 1 \quad (37)$$

Equation (28) can then be obtained by taking traces on both sides of (37). The AEKF-UI algorithm uses the variable weighting approach to compensate for the model error, which can lead to an improvement in both optimality and convergence. Furthermore, the proposed approach is efficient because of one-step forgetting factor update and has a moderate computational burden; therefore, it is convenient to implement for industrial applications. The overall flowchart of the AEKF-UI algorithm is shown in Figure 4.

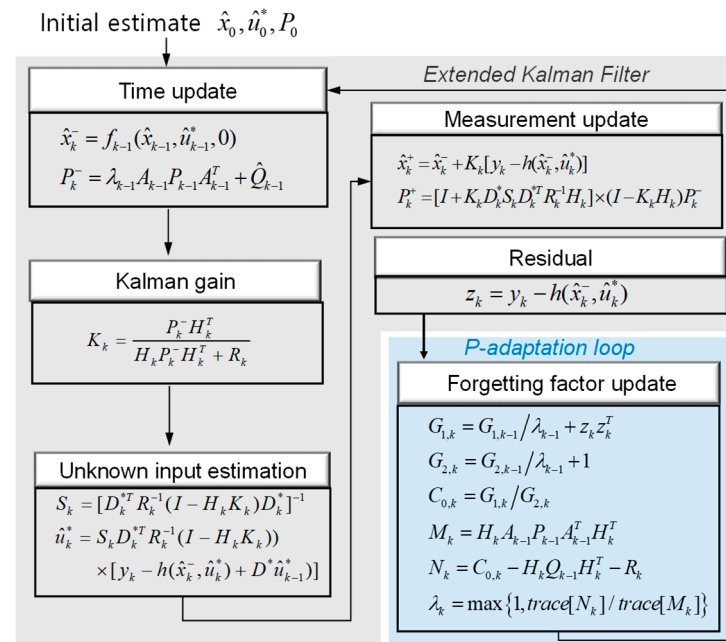


Figure 4. The overall flowchart of AEKF-UI algorithm with P-adaptation loop.

4. Simulation of AKEF-UI Algorithm

The simulation of the quarter-car suspension model was performed with the parameters listed in Table 2. In the embedded MATLAB function block, the signal x_r is used as an unknown road roughness input. According to the international roughness index (IRI), the road classification is based on different levels of its power spectral density function. In this study, the measured road roughness [30] was used to compare the estimated road roughness and evaluate its estimation performance. Figure 5 shows the road roughness input and its power spectral density function using Welch’s method regressed by a slope of -2.14 , which is close to the typical value (-2) of the smooth road roughness classified by IRI. Owing to the road input excitation, the vibration of the vehicle generated two acceleration signals (\ddot{x}_b and \ddot{x}_w) assumed to be measurable outputs in the simulation. The tire pressure drop scenario was set to suddenly decrease from 241.3 kPa (35 psi, normal) to 137.9 kPa (20 psi, abnormal) for 2.5 s (i.e., slew rate limited reference input) to imitate the under-inflated tire status, as shown in Figure 6. The vehicle was also assumed to be driven at a speed of 20 km/h and the simulation time was 40 s. The initial condition for state variable is set to be $x_0 = [0 \ 0 \ 0 \ 0 \ 220000]^T$ and the initial covariance matrix is set to be $P_0 = \text{diag}(1, 1, 1, 1, 10^5)$. The tuning of process and measurement noise covariance matrices in the random walk model is a critical step for Kalman filter algorithms [31]. The measurement noise covariance matrix is then tuned as to be $Q_k = 10^{-10} \cdot I_{5 \times 5}$ whereas the measurement noise covariance matrix is set to be constant $R_k = 0.5 \cdot I_{2 \times 2}$.

Table 2. Parameters for the simulation of the quarter-car suspension model and AEKF-UI.

Symbol	Parameters	Value
m_b	Sprung mass	240.8 kg
m_w	Unsprung mass	56.9 kg
c_s	Damping coefficient	925.8 N·s/m
k_s	Suspension spring constant	29114 N/m

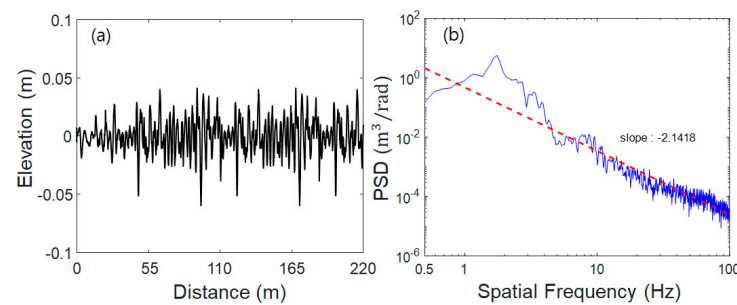


Figure 5. Unknown road roughness input for simulation; (a) measured road roughness at a vehicle speed of 20 km/h for 40 s and (b) its power spectral density function.

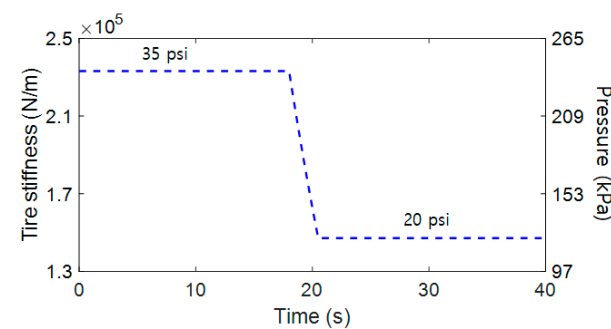


Figure 6. Tire pressure (i.e., stiffness) profile scenario for sudden pressure drop (241.3 kPa → 137.9 kPa).

The simulation results of the tire stiffness estimation are presented in Figure 7. The estimated tire stiffness by AEKF-UI shows a good transient response without significant delay in response to a sudden pressure drop whereas the EKF-UI is not capable of monitoring the sudden pressure drop. Because the goal of a TPMS is to prevent traffic accidents and increased tire rolling resistance due to under-inflated tires through early recognition of a lower tire pressure (abnormal) than threshold pressure (i.e., 30 psi, normal) of the tires, this quick transient behavior is sufficient for monitoring the sudden drop of tire pressure. In this study, the performance index of root mean square error (RMSE) is used to evaluate the tracking performance as follows [31]:

$$RMSE = \sqrt{\frac{1}{N} \sum_{k=1}^N (p(k) - \hat{p}(k))^2} = \sqrt{\frac{1}{N} \sum_{k=1}^N e(k)^2} \tag{38}$$

where N , $p(k)$ and $\hat{p}(k)$ are the length of simulation time instants, true pressure and indirect pressure estimation calculated from tire stiffness estimation using (5), respectively. $e(k)$ is the estimation error. The proposed algorithm can successfully track the tire stiffness with small tracking error (RMSE = 12.96), as shown in Figure 7c, whereas the EKF-UI fails to track the pressure, as shown in Figure 7a. The forgetting factor and error covariance of tire stiffness estimation were also adaptively updated in the neighborhood of pressure drop, as shown in Figure 7b,d. The proposed algorithm also simultaneously estimates the unknown road roughness input, as shown in Figure 8. Unlike most previous TPMS, AEKF-UI can

simultaneously estimate the time-varying parameter (tire stiffness) of vehicle suspension systems and the unknown road roughness input.

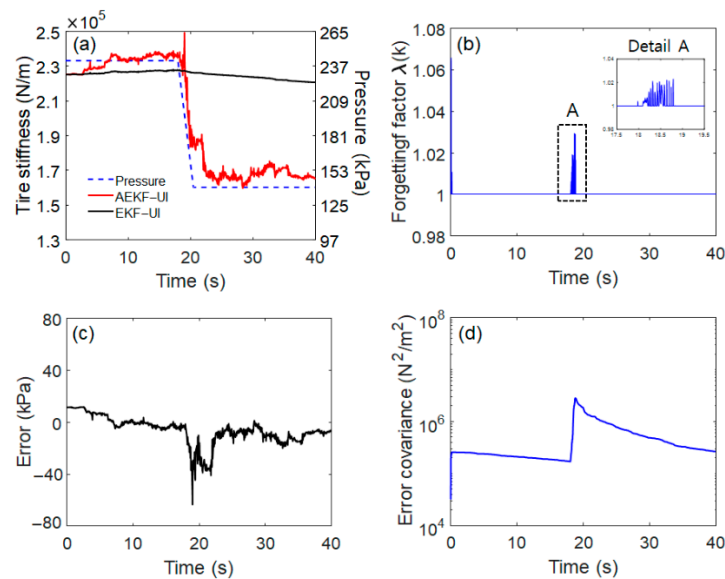


Figure 7. Simulation result of tire stiffness estimation; (a) responses of time-varying tire pressure to slow rate limited input (pressure drop), (b) time evolution of the forgetting factor (inset, detail around pressure change), (c) estimation error (AEKF–UI) and (d) convergence history of error covariance.

Various tire pressure change scenarios were applied to the simulation model to investigate the effectiveness of the proposed algorithm. These pressure change scenarios allow the evaluation of the accuracy of the proposed algorithm in estimating the parameter change under the same conditions such as process and measurement noise covariance matrices. The further pressure drop was set to be decreased from 241.3 kPa to 41.4 kPa for 2.5 s, as shown in Figure 9a. For arbitrary pressure change scenarios, the pressure starts to drop from 241.3 kPa to 138 kPa and recovered to 195 kPa, as shown in Figure 9b. If an active tire inflation system using a pneumatic pump is employed, this pressure change can be a potential pressure change scenario. Similar to Figure 7, the estimated tire stiffness and desired tire pressure show good agreement with small RMSE (23.21 for Figure 9a and 18.93 for Figure 9b).

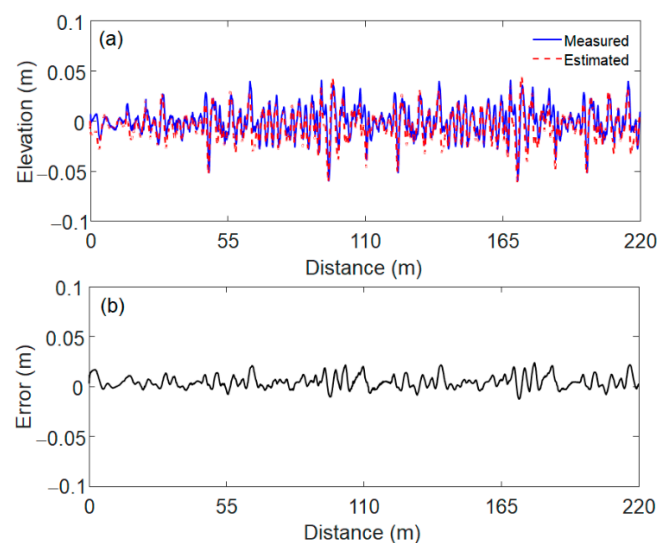


Figure 8. Simulation result of unknown road roughness input; (a) estimation of road roughness input, (b) estimation error between measured and estimated road roughness.

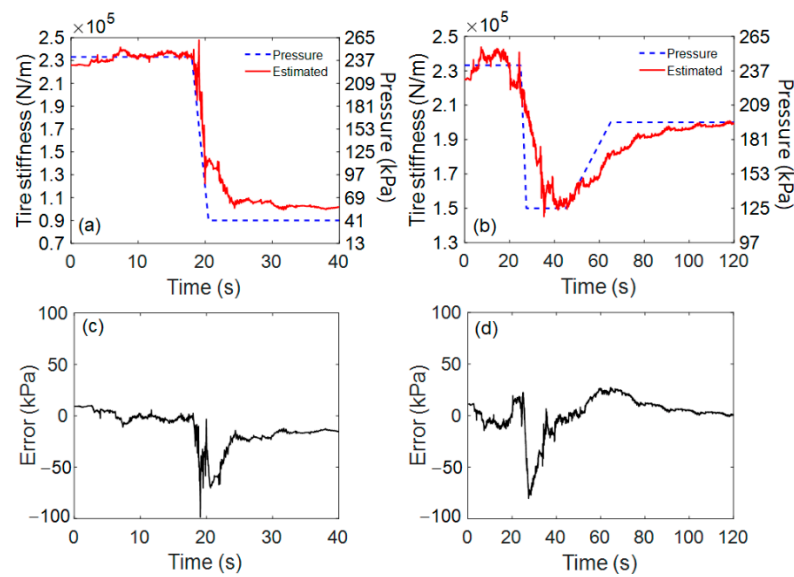


Figure 9. Simulation result of tire stiffness estimation with respect to different pressure drop scenarios; (a,c) time response of time-varying tire pressure to slow rate limited input (241.3 kPa → 41.4 kPa) and (b,d) time response for arbitrary pressure change (241.3 kPa → 138 kPa → 195 kPa).

In general, the Kalman filter is robust against mismatched process noise covariance due to parameter uncertainty [32,33]. Thus, the tire stiffness response of the quarter-car suspension model with variable sprung mass was examined to investigate the robustness of the proposed algorithm, because the variable sprung mass depends on the number of passengers and one of the significant model uncertainties (i.e., mismatched process noise). The nominal sprung mass of the suspension model (240 kg) was perturbed by -8% (220 kg) and 8% (260 kg), respectively, as shown in Figure 10a. The estimated tire stiffness and actual pressure input show good agreement. The simulation results show a good robustness against the model uncertainty such as the variation of sprung mass because the estimation error shows no significant changes, as listed in Table 3. Because of the P-adaptation, the magnitudes of the forgetting factor and error covariance for the perturbed sprung mass are more peaked compared to nominal (240 kg). The adaptive forgetting factor also allows the compensation of model parameter uncertainty due to variable sprung mass. The peak magnitude of error covariance histories is also closely related to the RMSE.

Table 3. Parameters for the simulation of the quarter-car suspension model and AEKF-UI.

Mass (kg)	RMSE	Relative Error to Nominal
220	17.57	35%
240 (nominal)	12.96	-
260	13.31	2.7%

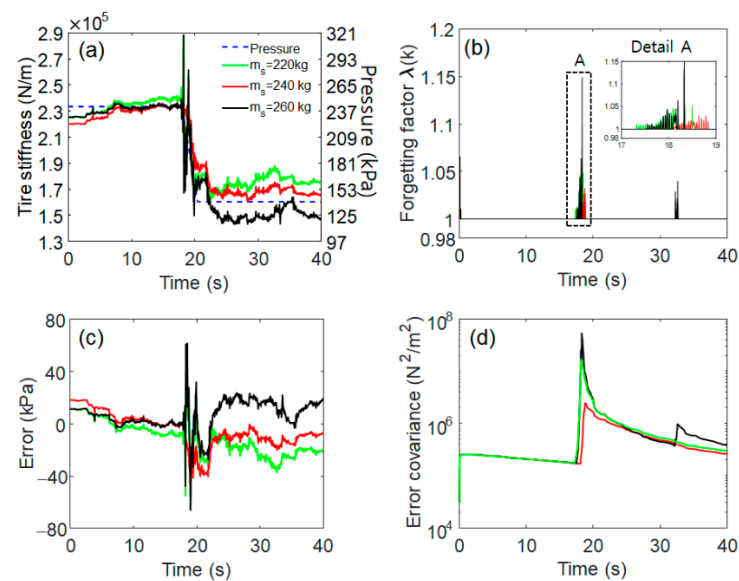


Figure 10. Simulation result of tire stiffness estimation with respect to different sprung masses. (a) Tire stiffness response to pressure drop (241.3 kPa \rightarrow 138 kPa), (b) time evolution of the forgetting factor (inset, detail around pressure change), (c) estimation error and (d) convergence history of error covariance.

5. Experimental Validation

5.1. Proof of Concept Experiment

As shown in Figure 11a, a laboratory-level test-bed was used as a quarter-car suspension and AEKF-UI was built in a real-time rapid control prototyping system (dSPACE®). The output signals, sprung and unsprung mass acceleration, were then measured by accelerometers and the AEKF-UI algorithm indirectly estimated the tire pressure. As shown in Figure 4, the forgetting factor updates the p-adaptation loop to adaptively change the error covariance matrix. A pressure sensor (PN2023, IFM electronics®), a ball valve and a pneumatic pump (NPK 09 DC, KNF®) were attached to the backside of the tire rim to measure and control the tire inflation pressure. The pressure starts to drop from 224 kPa to 142 kPa for 5 s, which is a rapid change compared to the normal situation, as shown in Figure 11b. The estimated pressure from the tire stiffness was compared with the actual pressure measured by a sensor. The random road profile was created by a hydraulic actuating system as a road input and the random segment is repeated every 0.66 s, which corresponds to 3.7 m with a vehicle speed assumed as 20 km/h. The linear variable differential transformer (LVDT) type position transducer (MTA-5E-5KC, Sensor solutions®) measured the road roughness profile segment, as shown in Figure 11c. Accelerometers (352C22, PCB®) were used to measure the sprung and unsprung mass acceleration. The spring and the damping coefficient were determined experimentally. The vertical load and displacement were measured to obtain spring stiffness and sinusoidal excitation was applied to determine the damping coefficient of the hydraulic damper. Based on these experiments, k_s and c_s are measured as 20,663 N/m and 435.2 N·s/m, respectively. The random road roughness for the experiment was generated using a hydraulic excitation unit. The initial values for the state variables are zero and the initial setup for the tire stiffness was 200,000 N/m (i.e., $x_0 = [0 \ 0 \ 0 \ 0 \ 200000]^T$). The error covariance matrix of the extended state vector was set to be $P_0 = \text{diag}(1, 1, 1, 1, 10)$. The covariance matrices of both the system noise vector w and the measurement noise vector v were set to be $Q_k = 10^{-8} \cdot I_{5 \times 5}$ and $R_k = 10 \cdot I_{2 \times 2}$, respectively.

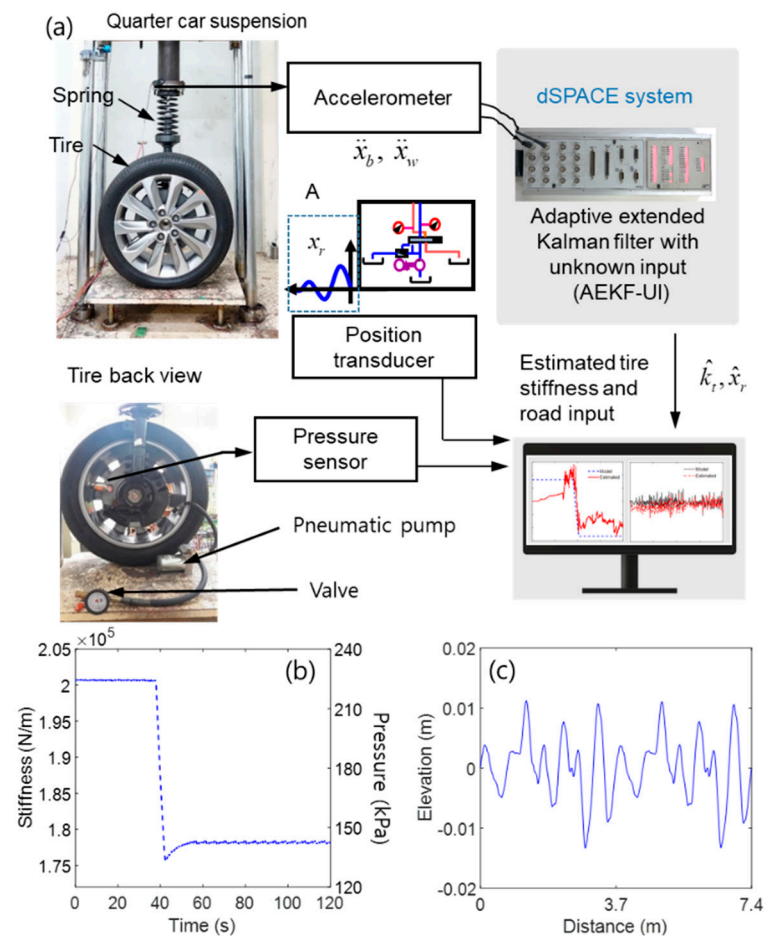


Figure 11. Experimental setup for indirect pressure measurements; (a) schematic diagram with photographs of quarter-car test-bed, (b) measured pressure drop scenario and (c) excited road roughness input (vehicle speed of 20 km/h).

The estimated tire stiffness using the proposed algorithm and the measured actual pressure are compared in Figure 12a. When the pressure suddenly drops from 224 kPa (normal) to 142 kPa (abnormal), the proposed algorithm can track this sudden drop in the inflation pressure and the tire pressure becomes steady-state (RMSE is 4.22). As the P-adaptation rule is applied to EKF-UI, the history of the error covariance matrix is examined to determine whether it has changed adaptively under optimality conditions. The forgetting factor history and the convergence history of error covariance in tire stiffness estimation are shown in Figure 12b,d. When the initial tire inflation pressure starts to drop from 38 s to 43 s, the error covariance is adaptively updated and eventually converges in real time because of the update of the forgetting factor calculated from (28). Figure 12d shows that the error covariance is weighted by the forgetting factor. The weighted error covariance matrix affects the time and measurement update process which results in time-varying parameter estimation.

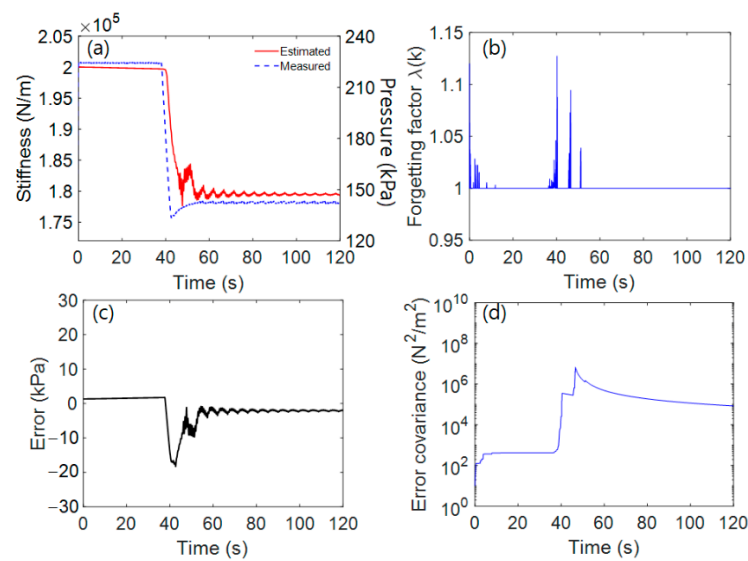


Figure 12. Experimental results of tire stiffness estimation; (a) response of time-varying tire stiffness to slow rate limited input (pressure drop), (b) time evolution of the forgetting factor, (c) estimation error and (d) convergence history of the error covariance.

To further investigate the effectiveness of proposed algorithm, different pressure profiles are employed. The tire pressure is set to be suddenly dropped from 224 kPa to 142 kPa (abnormal) and slowly recovered to 180 kPa by using a pneumatic pump. The tire pressure started to drop from 5 s to 10 s and slowly increased for 30 s, as shown in Figure 13a. Another pressure drop scenario was set to be gradually decreased from 220 kPa to 160 kPa for 30 s (i.e., different slow rate limited reference input) to represent the slow under-inflated tire status, as shown in Figure 13b. Although the estimated tire stiffness and desired tire pressure show some differences, these results seem to be acceptable for monitoring purposes.

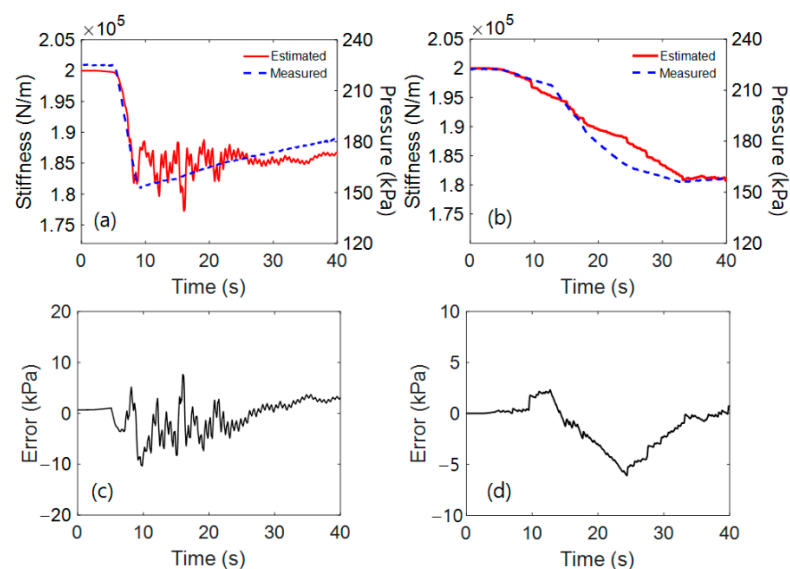


Figure 13. Experimental results of tire stiffness estimation; (a,c) tire stiffness estimation response and estimation error for sudden drop and slowly recovered pressure change (224 kPa → 142 kPa → 180 kPa), (b,d) response and estimation error for different slow rate limited reference input.

5.2. Robustness Analysis

To evaluate the robustness of the proposed algorithm, the RMSE for different sprung masses are analyzed and compared. The nominal sprung mass (240 kg) was perturbed

by 220 kg (−8%) and 260 kg (8%), respectively, which is same as simulation, as shown in Figure 14. The experimental results show a good robustness against the model uncertainty such as the variation of sprung mass because the estimation error shows no significant change, as listed in Table 4.

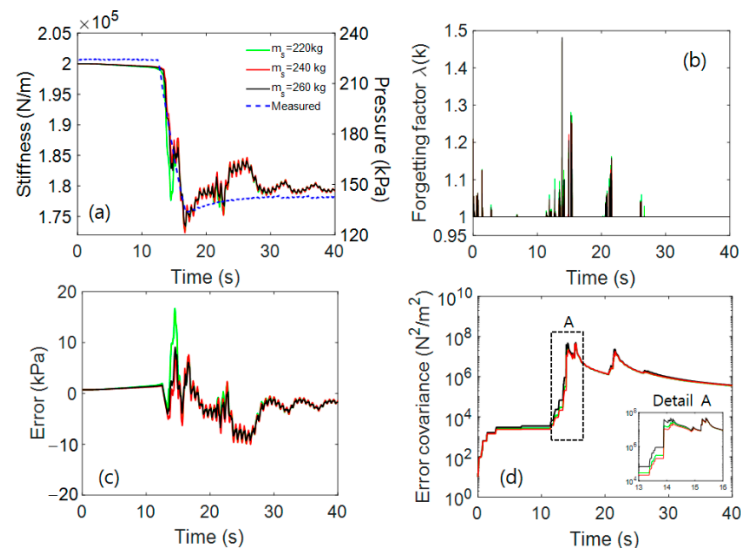


Figure 14. Experimental results of tire stiffness estimation with respect to different sprung mass; (a) response of time-varying tire stiffness, (b) time evolution of the forgetting factor, (c) estimation error and (d) convergence history of the error covariance (inset: detail A, around pressure change).

Table 4. Comparison of RMSE for different sprung masses.

Mass (kg)	RMSE	Relative Error to Nominal
220	3.48	9.7%
240 (nominal)	3.17	-
260	3.12	1.5%

To further illustrate the robustness of AEKF-UI, the effect of electrical noise on the estimation performance was examined [34]. The white Gaussian random noise was added to the measured acceleration of unsprung mass. Because the random noise (error) can be fitted to a normal Gaussian distribution with the variance $\sigma^2 = 0.248$, as shown in Figure 15b, it was confirmed by white Gaussian noise. An original random noise has been modified to produce the more contaminated Gaussian noise, as shown in Figure 15d ($\sigma^2 = 0.274$) and (f) ($\sigma^2 = 0.380$). The experimental results show a good robustness against the Gaussian random noise extracted from acceleration sensor signal, as shown in Figure 16. The estimation error shows no significant change, as listed in Table 5.

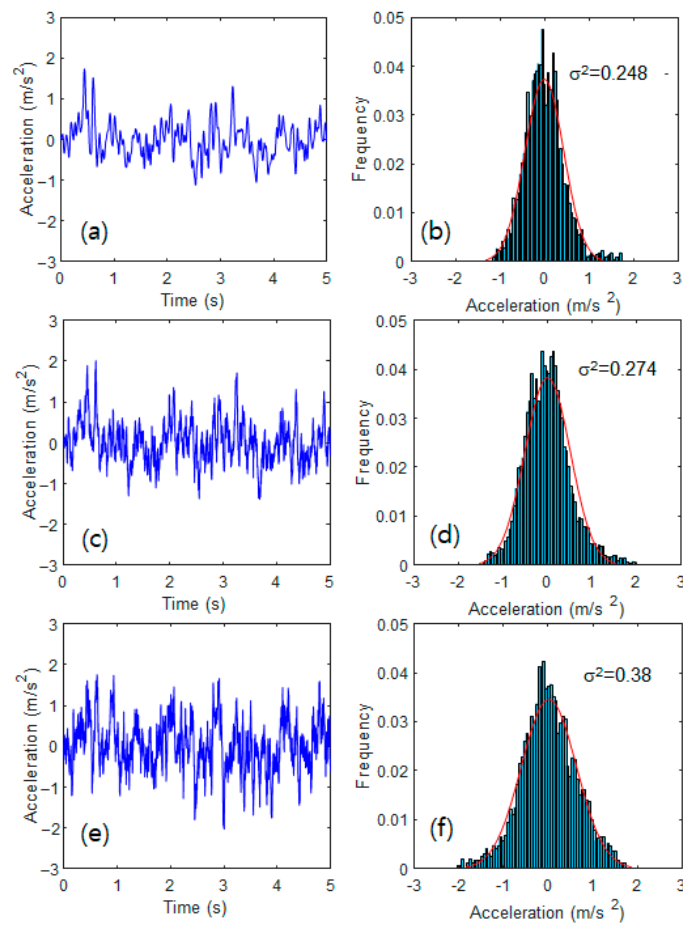


Figure 15. Gaussian random noises for robustness evaluation; (a,b) original extracted from the acceleration of unprung mass, (c,d) contaminated, (e,f) more contaminated.

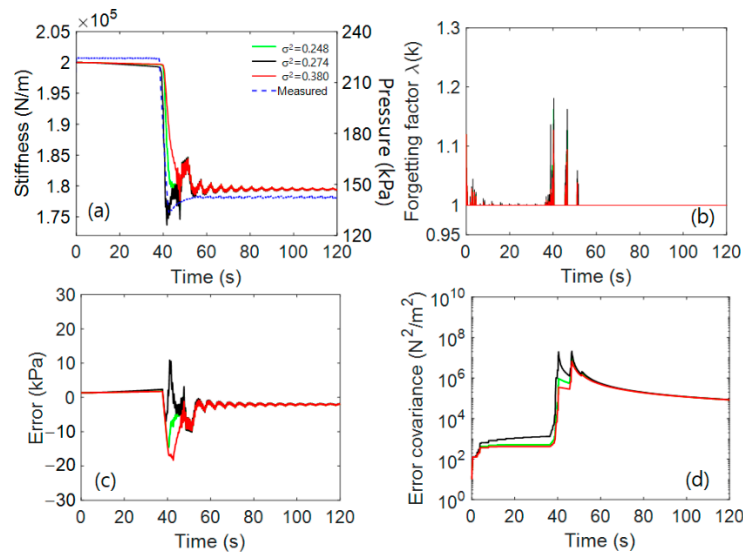


Figure 16. Experimental results of tire stiffness estimation for three data sets of Gaussian random noise; (a) response of time-varying tire stiffness to pressure drop with the sprung mass variation, (b) time evolution of the forgetting factor, (c) indirect pressure estimation error (nominal and perturbed sprung mass) and (d) convergence history of the error covariance (inset: detail A, around pressure change).

Table 5. Comparison of RMSE for different Gaussian random noises (variances).

Variance	RMSE	Relative Error to Nominal
0.248 (nominal)	3.02	-
0.274	2.67	11.58%
0.380	4.22	39%

6. Conclusions

In this study, an adaptive extended Kalman filter with unknown input was developed to estimate not only the tire stiffness for monitoring the inflation tire pressure indirectly but also the unknown road roughness input of the vehicle suspension system. The proposed algorithm is robust because it uses a weighting approach to compensate for errors in the uncertainty model. The analytical recursive solution for the proposed algorithm and the adaptive adjustment of the forgetting factor were successfully developed. We demonstrated that it is possible to simultaneously estimate the time-varying parameter of tire stiffness and unknown input through both simulation and experiment because the proposed algorithm can pick up a sudden drop in tire inflation pressure (such as when the pressure is sharply changed from the normal value of 224 kPa to the abnormal value of 142 kPa) and road roughness simultaneously. Although this indirect method of using sensor fusion technology offers possibilities for vehicular electronic applications for advanced TPMS and road roughness estimation, some technical issues remain to be further studied. The future direction of research includes the improvement of the proposed algorithm for the full-car suspension model (four individual stand-alone TPMS), the extension of the current proof-of-concept experiment to an in-vehicle test-bed equipped with real suspension system and the implementation of the proposed TPMS using a cost-effective embedded microcontroller. In particular, the proposed algorithm based on the simple quarter-car model should be experimentally evaluated in the future through in-vehicle tests because the nonlinear characteristics of suspension systems were neglected and approximately modeled by the linear quarter-car suspension model.

Author Contributions: G.-W.K. takes the primary responsibility for this research as the principal investigator and drafted the manuscript. D.-H.L. contributed to the analysis, algorithm, and writing of the manuscript. D.-S.Y. contributed to writing, editing, and experiment. All authors have read and agreed to the published version of the manuscript.

Funding: This work was supported by the INHA UNIVERSITY Research Grant.

Data Availability Statement: The data used to support the findings of this study are included within the article.

Acknowledgments: The authors would like to thank Jung-Sik Kim and Jeong-Heon Park for providing technical data on tire stiffness.

Conflicts of Interest: The authors declare no conflict of interest.

References

- Persson, N.; Gustafsson, F.; Drevö, M. Indirect tire pressure monitoring using sensor fusion. *SAE Trans.* **2002**, 1657–1662.
- Owende, P.M.; Hartman, A.M.; Ward, S.M.; Gilchrist, M.D.; O'Mahony, M.J. Minimizing distress on flexible pavements using variable tire pressure. *J. Transp. Eng.* **2001**, *127*, 254–262. [[CrossRef](#)]
- Kowalewski, M. Monitoring and managing tire pressure. *IEEE Potentials* **2004**, *23*, 8–10. [[CrossRef](#)]
- Wu, L.; Wang, Y.; Jia, C.; Zhang, C. Battery-less piezoceramics mode energy harvesting for automobile TPMS. In Proceedings of the 2009 IEEE 8th International Conference on ASIC, Changsha, China, 20–23 October 2009; pp. 1205–1208.
- Roundy, S. Energy harvesting for tire pressure monitoring systems: Design considerations. In Proceedings of the Power MEMS+ microMEMS, Sendai, Japan, 9–12 November 2008; pp. 9–12.
- Zhao, J.; Su, J.; Zhu, B.; Shan, J. An indirect TPMS algorithm based on tire resonance frequency estimated by AR model. *SAE Int. J. Passeng. Cars Mech. Syst.* **2016**, *9*, 99–106. [[CrossRef](#)]
- Silva, A.; Sánchez, J.R.; Granados, G.E.; Tudon-Martinez, J.C.; Lozoya-Santos, J.d.J. Comparative Analysis in Indirect Tire Pressure Monitoring Systems in Vehicles. *IFAC PapersOnLine* **2019**, *52*, 54–59. [[CrossRef](#)]

8. Isermann, R.; Wesemeier, D. Indirect vehicle tire pressure monitoring with wheel and suspension sensors. *IFAC Proc. Vol.* **2009**, *42*, 917–922. [[CrossRef](#)]
9. Han, J.; Sun, Y.; Tang, X. Research on tire pressure monitoring system based on the tire longitudinal stiffness. In Proceedings of the 2008 IEEE International Conference on Automation and Logistics, Qingdao, China, 1–3 September 2008; pp. 1648–1652.
10. Marton, Z.; Fodor, D.; Enisz, K.; Nagy, K. Frequency analysis based tire pressure monitoring. In Proceedings of the 2014 IEEE International Electric Vehicle Conference (IEVC), Florence, Italy, 17–19 December 2014; pp. 1–5.
11. Kang, S.-W.; Kim, J.-S.; Kim, G.-W. Road roughness estimation based on discrete Kalman filter with unknown input. *Veh. Syst. Dyn.* **2019**, *57*, 1530–1544. [[CrossRef](#)]
12. Kutluay, E.; Winner, H. Validation of vehicle dynamics simulation models—A review. *Veh. Syst. Dyn.* **2014**, *52*, 186–200. [[CrossRef](#)]
13. Yoon, D.-S.; Kim, G.-W.; Choi, S.-B. Response time of magnetorheological dampers to current inputs in a semi-active suspension system: Modeling, control and sensitivity analysis. *Mech. Syst. Signal Process.* **2021**, *146*, 106999. [[CrossRef](#)]
14. Türkay, S.; Akçay, H. A study of random vibration characteristics of the quarter-car model. *J. Sound Vib.* **2005**, *282*, 111–124. [[CrossRef](#)]
15. Hurel, J.; Mandow, A.; García-Cerezo, A. Kinematic and dynamic analysis of the McPherson suspension with a planar quarter-car model. *Veh. Syst. Dyn.* **2013**, *51*, 1422–1437. [[CrossRef](#)]
16. Maher, D.; Young, P. An insight into linear quarter car model accuracy. *Veh. Syst. Dyn.* **2011**, *49*, 463–480. [[CrossRef](#)]
17. Rangegowda, P.H.; Valluru, J.; Patwardhan, S.C.; Mukhopadhyay, S. Simultaneous state and parameter estimation using receding-horizon nonlinear kalman filter. *IFAC PapersOnLine* **2018**, *51*, 411–416. [[CrossRef](#)]
18. Ding, X.; Wang, Z.; Zhang, L.; Wang, C. Longitudinal Vehicle Speed Estimation for Four-Wheel-Independently-Actuated Electric Vehicles Based on Multi-Sensor Fusion. *IEEE Trans. Veh. Technol.* **2020**, *69*, 12797–12806. [[CrossRef](#)]
19. Wang, C.; Wang, Z.; Zhang, L.; Cao, D.; Dorrell, D.G. A Vehicle Rollover Evaluation System Based on Enabling State and Parameter Estimation. *IEEE Trans. Ind. Inform.* **2020**, *17*, 4003–4013. [[CrossRef](#)]
20. Taylor, R.; Bashford, L.; Schrock, M. Methods for measuring vertical tire stiffness. *Trans. ASAE* **2000**, *43*, 1415. [[CrossRef](#)]
21. Kalman, R.E. A new approach to linear filtering and prediction problems. *J. Basic Eng.* **1960**, *82*, 35–54. [[CrossRef](#)]
22. Gelb, A. Nonlinear Estimation. In *Applied Optimal Estimation*, 6th ed.; MIT Press: Cambridge, MA, USA, 1974; pp. 182–199.
23. Yang, J.N.; Lin, S.; Huang, H.; Zhou, L. An adaptive extended Kalman filter for structural damage identification. *Struct. Control Health Monit. Off. J. Int. Assoc. Struct. Control Monit. Eur. Assoc. Control Struct.* **2006**, *13*, 849–867. [[CrossRef](#)]
24. Xia, Q.; Rao, M.; Ying, Y.; Shen, X. Adaptive fading Kalman filter with an application. *Automatica* **1994**, *30*, 1333–1338. [[CrossRef](#)]
25. Lou, T.-S.; Wang, Z.-H.; Xiao, M.-L.; Fu, H.-M. Multiple adaptive fading Schmidt-Kalman filter for unknown bias. *Math. Probl. Eng.* **2014**, *2014*, 623930. [[CrossRef](#)]
26. Lin, J.W.; Betti, R.; Smyth, A.W.; Longman, R.W. On-line identification of non-linear hysteretic structural systems using a variable trace approach. *Earthq. Eng. Struct. Dyn.* **2001**, *30*, 1279–1303. [[CrossRef](#)]
27. Hoshiya, M.; Saito, E. Structural identification by extended Kalman filter. *J. Eng. Mech.* **1984**, *110*, 1757–1770. [[CrossRef](#)]
28. Yoshida, I. Damage detection using Monte Carlo filter based on non-Gaussian noises. In Proceedings of the 8th International Conference on Structural Safety and Reliability (ICOSSAR 2001), Newport Beach, CA, USA, 17–22 June 2001.
29. Loh, C.-H.; Lin, C.-Y.; Huang, C.-C. Time domain identification of frames under earthquake loadings. *J. Eng. Mech.* **2000**, *126*, 693–703. [[CrossRef](#)]
30. Kim, G.-W.; Kang, S.-W.; Kim, J.-S.; Oh, J.-S. Simultaneous estimation of state and unknown road roughness input for vehicle suspension control system based on discrete Kalman filter. *Proc. Inst. Mech. Eng. Part D J. Automob. Eng.* **2020**, *234*, 1610–1622. [[CrossRef](#)]
31. Varshney, D.; Bhushan, M.; Patwardhan, S.C. State and parameter estimation using extended Kitanidis Kalman filter. *J. Process Control* **2019**, *76*, 98–111. [[CrossRef](#)]
32. Ge, Q.; Shao, T.; Duan, Z.; Wen, C. Performance analysis of the Kalman filter with mismatched noise covariances. *IEEE Trans. Autom. Control* **2016**, *61*, 4014–4019. [[CrossRef](#)]
33. Huang, Z.; Du, P.; Kosterev, D.; Yang, B. Application of extended Kalman filter techniques for dynamic model parameter calibration. In Proceedings of the 2009 IEEE Power & Energy Society General Meeting (IEEE PES 2009), Calgary, AB, Canada, 26–30 July 2009; pp. 1–8.
34. Huang, C.; Wang, Z.; Zhao, Z.; Wang, L.; Lai, C.S.; Wang, D. Robustness evaluation of extended and unscented Kalman filter for battery state of charge estimation. *IEEE Access* **2018**, *6*, 27617–27628. [[CrossRef](#)]